Published in final edited form as:

Spine (Phila Pa 1976). 2014 February 1; 39(3): 198–206. doi:10.1097/BRS.0000000000000103.

Annular repair using high-density collagen gel; a rat-tail *in vivo* model

Peter Grunert, MD[1], **Brandon H Borde, BS**[2,†], **Katherine D Hudson, BS**[2], **Michael R Macielak, BS**[1], **Lawrence J Bonassar, PhD**[2,3], and **Roger Härtl, MD**[1,*]

[1]Weill Cornell Brain and Spine Institute, Department of Neurological Surgery, Weill Cornell Medical College, NY, NY

[2]Department of Biomedical Engineering, Cornell University

[3]Sibley School of Mechanical and Aerospace Engineering, Cornell University

Introduction

Repair of annular defects could significantly improve treatment of degenerative spinal diseases.[1] Open defects compromise the ability of the annulus fibrosus (AF) to contain nuclear tissue in the disc space, thereby increasing the likelihood of reherniation and progressive degeneration after discectomies.[2–6] Furthermore, there has been concern that annular puncture for therapeutic or diagnostic procedures accelerates the progression of degenerative disc disease and promotes nuclear tissue extrusion.[7] Successful treatment of puncture defects could inhibit these degenerative changes.

Annular defects persist because of the very limited intrinsic healing capability of the AF, which does not significantly improve upon simple mechanical closure.[1,8–11] As a result, several research groups have investigated using biological materials for annular repair.

Rigid implants have been studied by Vadala et al. using tissue-engineered AF constructs in vitro[12] and by Ledet EH using small intestinal submucosa in vivo.[13] Implanted submucosa tissue reduced degenerative changes after annulotomy in sheep spine.

Schek et al. have studied injectable biomaterials with genipin cross-linked fibrin hydrogels. Fibrin integrated with sections of human AF tissue, showing promising biomechanical and cell seeding properties in vitro.[14] Our group tested injectable high-density collagen (HDC) gels and found that HDC can partially restore mechanical function to a needle-punctured rat-tail AF in vitro.[15] However, no studies reported use of injectable biomaterials to treat annular defects in vivo.

Annular defects induced by needle puncture lead to predictable patterns of disc degeneration in the rat-tail spine.[16,17] In such models, degeneration is initiated by extrusion of nucleus

*Corresponding author: Roger Härtl, M.D., Associate Professor of Neurological Surgery, Department of Neurological Surgery, Weill Cornell Medical College, New York-Presbyterian Hospital, (Editorial correspondences to first author please), 525 East 68th Street, Box 99, New York, New York 10021. Telephone: (212) 746-1996; Fax: (212) 746-8947; roger@hartlmd.net.
†Author contributed equally to this study as first author

pulposus (NP) tissue through the puncture defect. Although the needle puncture model has been frequently used to test biological materials for IVD regeneration,[18–21] no study yet has used this model to investigate repair of induced defects to prevent disc degeneration.

The goal of our study was to evaluate the ability of HDC to repair a needle-puncture AF defect in the rat-tail spine. Specifically, we wanted to test whether injected HDC gel can prevent nuclear tissue extrusion and consequent IVD degeneration, as determined by histological and radiological outcomes. In addition, we assessed whether cross-linking of injected collagen influences the repair process. For that purpose, riboflavin (RF), a photoactive initiator of collagen cross-linking, was added in different concentrations. In the presented study, the rat-tail model was used to screen these various compositions of collagen gels.

Methods

Study groups

We used 42 male, 10–12 week-old, inbred, nude, athymic rats for this study. Animals were divided into four groups. The first group of 14 was needle-punctured and injected with HDC of 15mg/ml concentration. The second group of 16 was punctured and injected with RF cross-linked HDC (15mg/ml): nine with 0.25mM RF, and six with 0.5mM. A third group of six was punctured and left untreated to serve as control. All the animals in these three groups were sacrificed after five weeks. Tails were collected and used for histological analysis. A fourth group of six animals was sacrificed; tails were collected and subsequently needle-punctured and injected with HDC. This group was used to study the morphology and distribution of the collagen directly after injection.

All animals were euthanatized with carbon dioxide following standard protocol from the American Veterinary Medical Association.

The study was approved by and undertaken in accordance with guidelines outlined by the Hospital of Special Surgery Institutional Animal Care and Use Committee (IACUC) and New York State.

Collagen gel preparation

Collagen was harvested and reconstituted from rat-tail tendon as previously described.[22,23] Fibers were digested in 0.1% acetic acid, frozen for 48 hours, lyophilized and reconstituted at 20mg/ml in 0.1% acetic acid. Immediately before delivery, acidic collagen solutions were mixed with working solutions consisting of 10× Dulbecco’s Phosphate Buffered Saline (DPBS), 1N NaOH and 1× DPBS to initiate polymerization of final collagen gels at 15mg/ml. For RF groups, riboflavin was added to 1× DPBS at the desired concentration. Gels with RF were exposed to blue light with a 480nm wavelength for 40 sec after injection to initiate cross-linking.

Open needle puncture and collagen injection

The target level between the 3rd and 4th vertebra of the tail was localized under X-ray control. The animals were anesthetized and placed in the prone position. A 2cm longitudinal

skin incision was made over the marked level. The AF was then exposed, and great care was taken to preserve it without damage. Subsequently the AF was punctured using an 18-gauge needle attached to a syringe containing the collagen gel. Approximately 0.5 ml of the gel was injected around the defect immediately after puncture. When RF was added to the collagen, the gel was cured in situ. The control group was punctured and left untreated. In order to standardize the puncture technique the needle was always inserted in the same orientation (with the needle bevel up) and to the same depth (until the bevel completely penetrated the AF).

Quantitative MR Imaging

Quantitative imaging was utilized to assess the size of the NP according to the number of MRI voxels that composed it, here labeled NP voxel count. MR imaging was obtained on a 7T MRI (Bruker 7T USR Preclinical MRI System) at one, two and five weeks post puncture (Fig. 1A).

We used a sagittal multi-slice multi-echo (MSME) pulse sequence (TR=2000ms, TE=12ms, NEX=2, number of echoes=12, echo spacing=12ms, slice thickness=1mm and matrix size=320 × 320, resolution: 125μm × 125μm × 1mm) to create a T2 map based upon fitting semi-log plots of T2 signal intensity versus relaxation time for the twelve acquired echoes. Bruker's proprietary program TopSpin™ was used for the fitting process. A color map was assigned to the resulting T2 map (Fig 1B). Next, a standard region of interest (ROI) measuring ~1mm^2 was drawn within the center of NP of the healthy disc proximal to the punctured IVD. The average T2-RT of that ROI was measured, and this value minus two standard deviations was used to set a subtraction threshold for all voxels in that slice (Fig. 1B). Voxels with T2 values lower than the threshold were subsequently subtracted (Fig. 1C). As a result, only voxels with T2 values representing NP tissue remained in the disc space and were then counted. At each time point, the mean voxel count of punctured discs was compared to the mean voxel count of proximal adjacent healthy IVDs.

Qualitative MRI analysis

A sagittal TurboRare sequence (TR=2017, ms, TE=60ms, NEX=6, echo train length=12, slice thickness=1mm and matrix size=320 × 320, resolution: 125μm × 125μm × 1mm) was utilized for qualitative assessments. We used a modified Pfirrmann scale[24] that outlines four grades of degeneration as defined by NP signal intensity, homogeneity and loss of disc height (Table 1).

Disc height measurements

Disc heights were obtained in a digital radiographic cabinet. Great care was taken to achieve true lateral X-rays of the index segment. The IVD height was expressed as a disc height index (DHI), calculated by dividing disc height by adjacent vertebral body height based on the modified method of Lu et al.[25] The disc height was measured preoperatively and postoperatively at one, two and five week time points.

Histology

After appropriate fixation, tails were decalcified, cut mid-sagittally and transferred to 75% ethanol. Segments were embedded in paraffin, then cut to 5μm thickness and stained with Alcian Blue and Safranin-O. We measured the size of the NP by drawing a ROI around the nucleus and subsequently measured the cross-sectional area of that ROI using the Bioquant image program (Fig. 2). The average cross-sectional area measurements of punctured discs were compared to those of healthy proximal adjacent IVDs. The Han grading system was used to describe the degenerative stage of the punctured IVDs. This system is based on AF/NP cellularity, morphology and border.[17] The grading system ranges from 5, a healthy disc, to 15, a terminally degenerated disc.

Statistics

The NP voxel count and disc height data were evaluated using nested multilevel ANOVA modeling with nesting in punctured and healthy adjacent levels, untreated puncture versus collagen injection, and riboflavin concentrations. Analysis was done in JMP 9.0 (SAS Institute Inc.). We considered $p \leq 0.05$ indicated a statistically significant correlation between the variables and measured outcomes.

Results

Qualitative MRI

Five out of six animals in the 0.5mM riboflavin group showed no obvious signs of degenerative changes at the five week MRI (Fig. 2). The modified Pfirrmann Grade of that group ranged from I to III (avg. 1.3). At the same time point, all animals in the 0.25mM riboflavin group displayed decreased NP size, yet the nucleus remained homogenous and hyperintense (Fig. 2). The Pfirrmann grade ranged from II to III (avg. 2.6). The uncross-linked collagen group showed a more heterogeneous, smaller NP with a significantly increased AF/NP ratio (Fig. 2). The AF bulged into the nucleus giving it an hourglass shape. All animals had a Pfirrmann grade of III. Five out of six specimens in the untreated group showed black IVDs, indicating terminal disc degeneration (Fig. 2). The Pfirrmann grade ranged from III to IV (avg. 3.8).

NP voxel count

The control IVDs had an average NP voxel count ranging from 140 to 153 voxels at 1, 2 and 5 weeks; the voxel count for the 0.5mM RF group was between 129 (SD±16.3) and 140 (SD ±22.5). The 0.25mM RF group exhibited lower values: 71 voxels (SD±59.14) at week one and 57 (SD±56.40) at the second and fifth weeks. The NP voxel counts of both RF groups remained constant between weeks two and five.

The uncross-linked collagen group showed 46 (SD±25) voxels at week one which continuously dropped to 14 (SD±15.6) at week five. The untreated group showed the lowest voxel counts values at each time point, decreasing to 5 (SD±4.17) after five weeks (Fig. 3A). Overall, HDC gel injection significantly increased voxel count values ($p<0.0001$) as

compared to untreated discs. Increasing RF concentration (0mM, 0.25mM, 0.5mM) proved to significantly increase NP voxel count values ($p<0.0001$).

Disc height measurements

All punctured IVDs dropped in disc height after needle puncture but remained constant between weeks two and five (Fig. 3B). The 0.5mM group maintained an average of 84% (SD±8.77) of its initial disc height, the 0.25mM riboflavin group 77% (SD±8.72).

The uncross-linked collagen group maintained 67% (SD±16.86) and the untreated group 53% (SD±13.82) of disc height. Overall, HDC treatment gel significantly improved the DHI ($p<0.0001$) of punctured discs. Increasing RF concentration (0mM, 0.25mM, 0.5mM) significantly increased the DHI ($p = 0.0264$).

Histology

The annular defect—The needle puncture defect pierced through all AF lamella layers (Fig. 4A–B, 5A–C) and was still visible after five weeks in all animals. In the control and uncross-linked groups, the AF fibers remained separated, and infiltrated the surrounding scar tissue (Fig. 4D). No granulation tissue, increased cellularity or vascularity was visible to indicate an annular repair process. The 0.5mM RF group showed formation of a fibrous cap at the outer third of the AF that infiltrated annular fibers, bridging both disrupted ends (Fig. 5). This fibrous cap was composed of fibroblasts embedded in a dense collagen matrix that stained more intensely with Safranin-O and Alcian blue than surrounding AF and scar tissue. The 0.25mM RF group showed formation of either a similar cap (Fig. 4A–B) or a thin fibrous string repairing the outer part of the AF (Fig. 4C). In both cross-linked groups, the inner two thirds of the AF showed no signs of tissue repair.

Disc degeneration—There were no obvious signs of degeneration in the 0.5mM RF group. IVDs showed an average Han degeneration grade of 6.8.

IVDs in the 0.25mM RF group showed a decline in NP cells with clusters formation, and reached an average Han grade of 9.3.

All IVDs in the uncross-linked collage group showed signs of progressed degenerative changes with only residual NP tissue visible in the disc space (Fig. 2). The puncture defect branched into the AF, creating multiple fissures. NP tissue herniated through the open defect (Fig. 4E). Discs a showed a Han grade of 12.8.

All animals in the untreated group showed severe signs of degeneration; the NP was completely replaced with connective tissue. The AF appeared ruptured and disorganized (Fig. 4F). Several specimens showed significant endplate damage (Fig. 2). The average Han grade was 14.3.

Histological cross-sectional area—After five weeks, healthy NP proximal to punctured IVDs had an average NP cross-sectional area of $1.59mm^2$. Means of 0.5mM RF, 0.25mM RF, and uncross-linked collagen groups were $1.29mm^2$, $0.78mm^2$, and $0.78mm^2$ respectively. No measurable NP tissue remained in the disc space of untreated IVDs.

Fate of the injected collagen

Immediately after injection, the collagen distributed into the paravertebral space covering the outer part of the annular defect but did not migrate into the defect (Fig. 6). HDC appeared as homogenous amorphous tissue that stained weakly with Alcian Blue or Safranin-O. After five weeks residual collagen still appeared homogenous and amorphous and was infiltrated with host fibroblasts to varying degrees. Resorptive zones were visible, indicating reorganization of the injected material by the host cells (Fig. 7). No sign of inflammatory or foreign body reaction was visible.

Discussion

Summary of our results

The first objective of this study was to test the ability of HDC to repair annular defects in a needle-punctured rat-tail model. We found that collagen can preserve the ability of the AF to retain nuclear tissue in the disc space and thereby prevent degenerative changes to the IVD. We also observed the potential of collagen gel to induce formation of fibrous tissue that partially restores annular integrity. The second objective was to evaluate whether adding RF affects the quality of AF repair. We found that RF improved retention of NP size and disc height for up to five weeks after needle puncture.

The beneficial effect of RF was dose-dependent. In its absence, collagen gels yielded only a nominal increase in NP size and disc height compared to untreated IVDs. The 0.5mM RF group retained most of its nuclear tissue according to NP voxel counts and histological cross-sectional area measurements. An average disc height of 84% was maintained. Neither MRI analysis nor histological assessment revealed significant degenerative changes.

There are several potential mechanisms by which cross-linking may have positively influenced AF repair. Chemical cross-linking is known to increase the stiffness and decrease the hydraulic permeability of collagen gels.[26–28] Increased stiffness may help form a more robust barrier for sealing the defect. Decreased hydraulic permeability limits the loss of highly hydrated NP material through the defect.[15] In addition, cross-linking may enhance collagen adhesion to the AF tissue as has been shown with other biopolymer gels.[14] This prevents detachment of the implanted material from the annulus and subsequent loss of NP tissue.

A notable histological finding was the formation of a fibrous cap bridging the outer portion of the annular defect in both cross-linked groups. Collagen gel showed varying degrees of host fibroblast infiltration with signs of tissue reorganization, which could explain the formation of this fibrous tissue. The mechanism of host cell invasion with subsequent tissue remodeling of collagen gels has already been described in the literature.[29,30] Staskowski et al. injected type I collagen gel in a canine model and described that secondary fibroblast invasion led to deposition of new host collagen within the gel. According to his study, cellular infiltration progressed more rapidly in a cross-linked collagen preparation, which could explain why fibrous cap formation occurred only in cross-linked groups of the presented study. Further, cross-linking is known to delay degradation and increase

persistence time of collagen scaffolds, which would also support cell migration and remodeling.[31,32]

RF cross-linking and injectable biomaterials

RF is already used clinically to cross-link collagen fibers of the cornea to treat keratoconus,[33] but has never been applied to repair IVD tissue.

RF serves as a photosensitizer to induce production of oxygen radicals, which then induce chemical bonds between collagen fibrils, thereby cross-linking them.[28] Several different substances have been used to cross-link biopolymer gels.[14,31,32] Using RF is advantageous because it cross-links fibers only after activation by blue light in situ, allowing collagen gel to remain liquid prior to injection. Injectable biomaterials may prove more technically feasible for use in spinal procedures than rigid biological implants, as they do not require anchoring to the AF or vertebral body. Moreover, only injectable substances can be applied percutaneusly.

The rat-tail model

The rat-tail model proved to be suitable for testing various compositions of collagen gels. An 18-gauge needle creates a large defect comprising almost the entire posterior wall of the AF in the rat-tail disc. This defect is proportionally much larger than defects induced by annulotomy during discectomies or punctures for discographies. High intradiscal pressure combined with the liquid consistency of the NP leads to rapid extrusion of nuclear tissue if left untreated.

Untreated IVDs degenerated more rapidly than described in other studies that used the same model with a percutaneous approach.[16] We believe this is due to the open approach used in our study, in which the paravertebral muscles are dissected off the AF, creating a large tissue defect.

Limitations

We consider the small size of the specimen to be the main limitation of this study. The relatively small IVDs did not allow us to inject collagen gel into deeper layers of the AF against the intra discal pressure. As a result, the potential of collagen gel to repair deeper layers of the AF could not be studied. It is unclear if the described fibrous cap at the outer part of the annulus could mechanically compensate for defects in larger animals or humans whose IVDs are exposed to much higher mechanical forces. In addition, the instantaneous sealing of the defect by the injected collagen could be less effective under higher axial loads in humans. One other limitation of this model is that the AF is not degenerated at the time of collagen injection. A degenerated AF, as often seen in discectomy procedures, might respond differently to the collagen gel.

However, the potential of collagen gel to induce tissue repair is very promising and should be explored in degenerated discs and larger animals.

Conclusion

High-density type I collagen is able to repair annular defects for up to five weeks after induction of a needle-puncture defect in the AF of the rat-tail spine. This capability correlates positively with RF cross-linking. The needle-punctured rat-tail has been shown to be a suitable in vivo model for studying biomaterials for annular repair. Testing different concentrations of RF in longer-term studies will be an important next step. Additionally, future experiments may look to increase the size of the animal model or to incorporate cell-loading of the collagen gel.

Supplementary Material

Refer to Web version on PubMed Central for supplementary material.

Acknowledgments

We express our gratitude to AOSpine North America for their support with fellowship funding for Peter Grunert. We thank Stephen Doty PhD, for his work on the histology. We would also like to thank Sara Towne for her tremendous help with writing and reviewing this paper.

The manuscript submitted does not contain information about medical device(s)/drug(s). AO Research Fund Grant F-08-10B, the AOSpine International Hansjörg Wyss Focus Award 2010, and a grant from NFL Medical Charities funds were received in support of this work. Relevant financial activities outside the submitted work: grants.

References

1. Bron JL, Helder MN, Meisel HJ, et al. Repair, regenerative and supportive therapies of the annulus fibrosus: achievements and challenges. Eur Spine J. 2009; 18:301–13. [PubMed: 19104850]
2. Lebow RL, Adogwa O, Parker SL, et al. Asymptomatic same-site recurrent disc herniation after lumbar discectomy: results of a prospective longitudinal study with 2-year serial imaging. Spine. 2011; 36:2147–51. [PubMed: 21343849]
3. Ambrossi GL, McGirt MJ, Sciubba DM, et al. Recurrent lumbar disc herniation after single-level lumbar discectomy: incidence and health care cost analysis. Neurosurgery. 2009; 65:574–8. discussion 8. [PubMed: 19687703]
4. McGirt MJ, Eustacchio S, Varga P, et al. A prospective cohort study of close interval computed tomography and magnetic resonance imaging after primary lumbar discectomy: factors associated with recurrent disc herniation and disc height loss. Spine. 2009; 34:2044–51. [PubMed: 19730212]
5. Carragee EJ, Spinnickie AO, Alamin TF, et al. A prospective controlled study of limited versus subtotal posterior discectomy: short-term outcomes in patients with herniated lumbar intervertebral discs and large posterior anular defect. Spine. 2006; 31:653–7. [PubMed: 16540869]
6. Carragee EJ, Han MY, Suen PW, et al. Clinical outcomes after lumbar discectomy for sciatica: the effects of fragment type and anular competence. J Bone Joint Surg Am. 2003; 85-A:102–8. [PubMed: 12533579]
7. Carragee EJ, Don AS, Hurwitz EL, et al. 2009 ISSLS Prize Winner: Does discography cause accelerated progression of degeneration changes in the lumbar disc: a ten-year matched cohort study. Spine. 2009; 34:2338–45. [PubMed: 19755936]
8. Melrose J, Smith SM, Little CB, et al. Recent advances in annular pathobiology provide insights into rim-lesion mediated intervertebral disc degeneration and potential new approaches to annular repair strategies. European spine journal: official publication of the European Spine Society, the European Spinal Deformity Society, and the European Section of the Cervical Spine Research Society. 2008; 17:1131–48.

9. Bron JL, van der Veen AJ, Helder MN, et al. Biomechanical and in vivo evaluation of experimental closure devices of the annulus fibrosus designed for a goat nucleus replacement model. Eur Spine J. 2010; 19:1347–55. [PubMed: 20401620]
10. Fazzalari NL, Costi JJ, Hearn TC, et al. Mechanical and pathologic consequences of induced concentric anular tears in an ovine model. Spine. 2001; 26:2575–81. [PubMed: 11725238]
11. Hampton D, Laros G, McCarron R, et al. Healing potential of the anulus fibrosus. Spine. 1989; 14:398–401. [PubMed: 2718042]
12. Vadala G, Mozetic P, Rainer A, et al. Bioactive electrospun scaffold for annulus fibrosus repair and regeneration. Eur Spine J. 2012; 21(Suppl 1):S20–6. [PubMed: 22411039]
13. Ledet EH, Jeshuran W, Glennon JC, et al. Small intestinal submucosa for anular defect closure: long-term response in an in vivo sheep model. Spine. 2009; 34:1457–63. [PubMed: 19525836]
14. Schek RM, Michalek AJ, Iatridis JC. Genipin-crosslinked fibrin hydrogels as a potential adhesive to augment intervertebral disc annulus repair. Eur Cell Mater. 2011; 21:373–83. [PubMed: 21503869]
15. Borde, BH.; James, AR.; Härtl, R., et al. Repair of Defects in the Rat Tail Annulus Fibrosus Using Injectable High Density Collagen Gels; Orthopedic Research Society, ANNUAL MEETING 2012; San Francisco, CA. 2012.
16. Keorochana G, Johnson JS, Taghavi CE, et al. The effect of needle size inducing degeneration in the rat caudal disc: evaluation using radiograph, magnetic resonance imaging, histology, and immunohistochemistry. Spine J. 2010; 10:1014–23. [PubMed: 20970740]
17. Han B, Zhu K, Li FC, et al. A simple disc degeneration model induced by percutaneous needle puncture in the rat tail. Spine. 2008; 33:1925–34. [PubMed: 18708924]
18. Zou F, Jiang J, Lu F, et al. Efficacy of intradiscal hepatocyte growth factor injection for the treatment of intervertebral disc degeneration. Mol Med Rep. 2013; 8:118–22. [PubMed: 23632892]
19. Zhang H, Wang L, Park JB, et al. Intradiscal injection of simvastatin retards progression of intervertebral disc degeneration induced by stab injury. Arthritis Res Ther. 2009; 11:R172. [PubMed: 19912653]
20. Gullung GB, Woodall JW, Tucci MA, et al. Platelet-rich plasma effects on degenerative disc disease: analysis of histology and imaging in an animal model. Evid Based Spine Care J. 2011; 2:13–8. [PubMed: 23230401]
21. Sheikh H, Zakharian K, De La Torre RP, et al. In vivo intervertebral disc regeneration using stem cell-derived chondroprogenitors. J Neurosurg Spine. 2009; 10:265–72. [PubMed: 19320588]
22. Cross VL, Zheng Y, Won Choi N, et al. Dense type I collagen matrices that support cellular remodeling and microfabrication for studies of tumor angiogenesis and vasculogenesis in vitro. Biomaterials. 2010; 31:8596–607. [PubMed: 20727585]
23. Bowles RD, Williams RM, Zipfel WR, et al. Self-assembly of aligned tissue-engineered annulus fibrosus and intervertebral disc composite via collagen gel contraction. Tissue Eng Part A. 2010; 16:1339–48. [PubMed: 19905878]
24. Yu LP, Qian WW, Yin GY, et al. MRI assessment of lumbar intervertebral disc degeneration with lumbar degenerative disease using the Pfirrmann grading systems. PLoS One. 2012; 7:e48074. [PubMed: 23284612]
25. Lu DS, Shono Y, Oda I, et al. Effects of chondroitinase ABC and chymopapain on spinal motion segment biomechanics. An in vivo biomechanical, radiologic, and histologic canine study. Spine. 1997; 22:1828–34. discussion 34–5. [PubMed: 9280018]
26. Cheng NC, Estes BT, Young TH, et al. Genipin-crosslinked cartilage-derived matrix as a scaffold for human adipose-derived stem cell chondrogenesis. Tissue Eng Part A. 2013; 19:484–96. [PubMed: 23088537]
27. Stewart JM, Schultz DS, Lee OT, et al. Collagen cross-links reduce corneal permeability. Invest Ophthalmol Vis Sci. 2009; 50:1606–12. [PubMed: 19060268]
28. Tirella A, Liberto T, Ahluwalia A. Riboflavin and collagen: New crosslinking methods to tailor the stiffness of hydrogels. Materials Letters. 2012; 74:58–61.
29. Guidry C, Grinnell F. Studies on the mechanism of hydrated collagen gel reorganization by human skin fibroblasts. J Cell Sci. 1985; 79:67–81. [PubMed: 3914484]

30. Staskowski PA, Ford CN, Inagi K. The histologic fate of autologous collagen injected into the canine vocal fold. Otolaryngol Head Neck Surg. 1998; 118:187–90. [PubMed: 9482550]

31. Harriger MD, Supp AP, Warden GD, et al. Glutaraldehyde crosslinking of collagen substrates inhibits degradation in skin substitutes grafted to athymic mice. J Biomed Mater Res. 1997; 35:137–45. [PubMed: 9135162]

32. Jarman-Smith ML, Bodamyali T, Stevens C, et al. Porcine collagen crosslinking, degradation and its capability for fibroblast adhesion and proliferation. J Mater Sci Mater Med. 2004; 15:925–32. [PubMed: 15477745]

33. Hashemi H, Seyedian MA, Miraftab M, et al. Corneal Collagen Cross-linking with Riboflavin and Ultraviolet A Irradiation for Keratoconus: Long-term Results. Ophthalmology. 2013

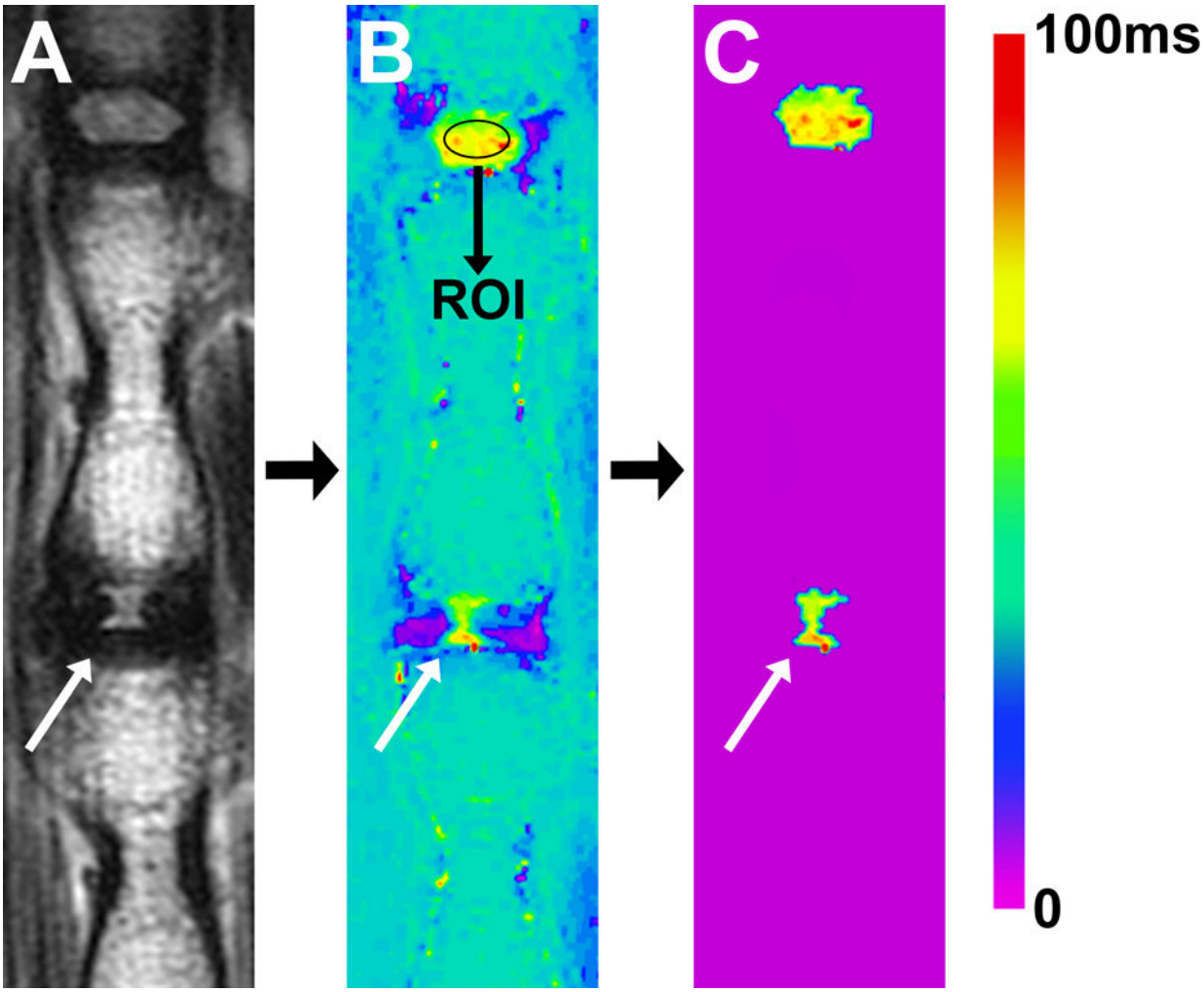

Fig. 1.

Illustrating the method used to determine NP size according to T2-RT. **(A)** T2-weighted MRI of a rat-tail with a needle-punctured disc (white arrow). **(B)** Matching image with T2-RT measurements displayed as a color map. A ROI was drawn within the NP of the proximal healthy adjacent disc. A subtraction threshold was set at two standard deviations below the T2-RT mean of the ROI. **(C)** All voxels below the threshold were subtracted. Subsequently, the remaining voxels in the disc space were counted.

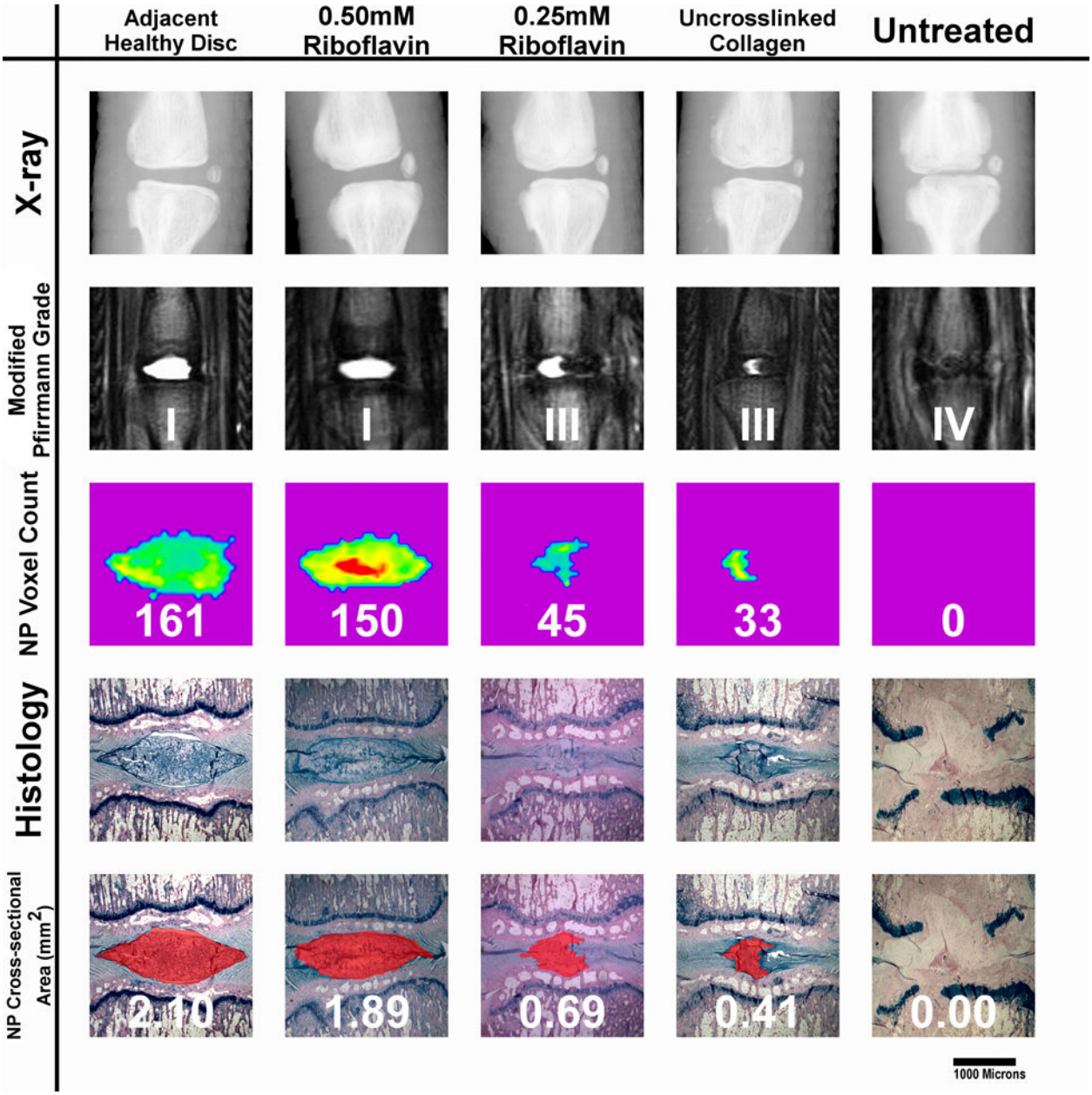

Fig. 2.

Five-week outcome examples of all punctured groups. The displayed specimen from the **0.5mM RF group** shows only a slight reduction in NP size when compared to healthy discs, according to the NP voxel count and histological cross-section measurements. The IVD from the **0.25RF group** shows a reduced nuclear size. The NP appears still homogeneous and hyperintense but has lost its oval shape. The decreased disc height, which is also seen on X-Ray, results in a Pfirrmann grade of III. The **uncross-linked** collagen injected IVD shows a greater reduction in NP size. The NP is still hyperintense but appears more heterogeneous. **The untreated disc** shows terminal degenerative changes: a black disc on MRI combined with collapsed disc space. The NP tissue has been completely replaced with connective tissue. Endplate damage is visible.

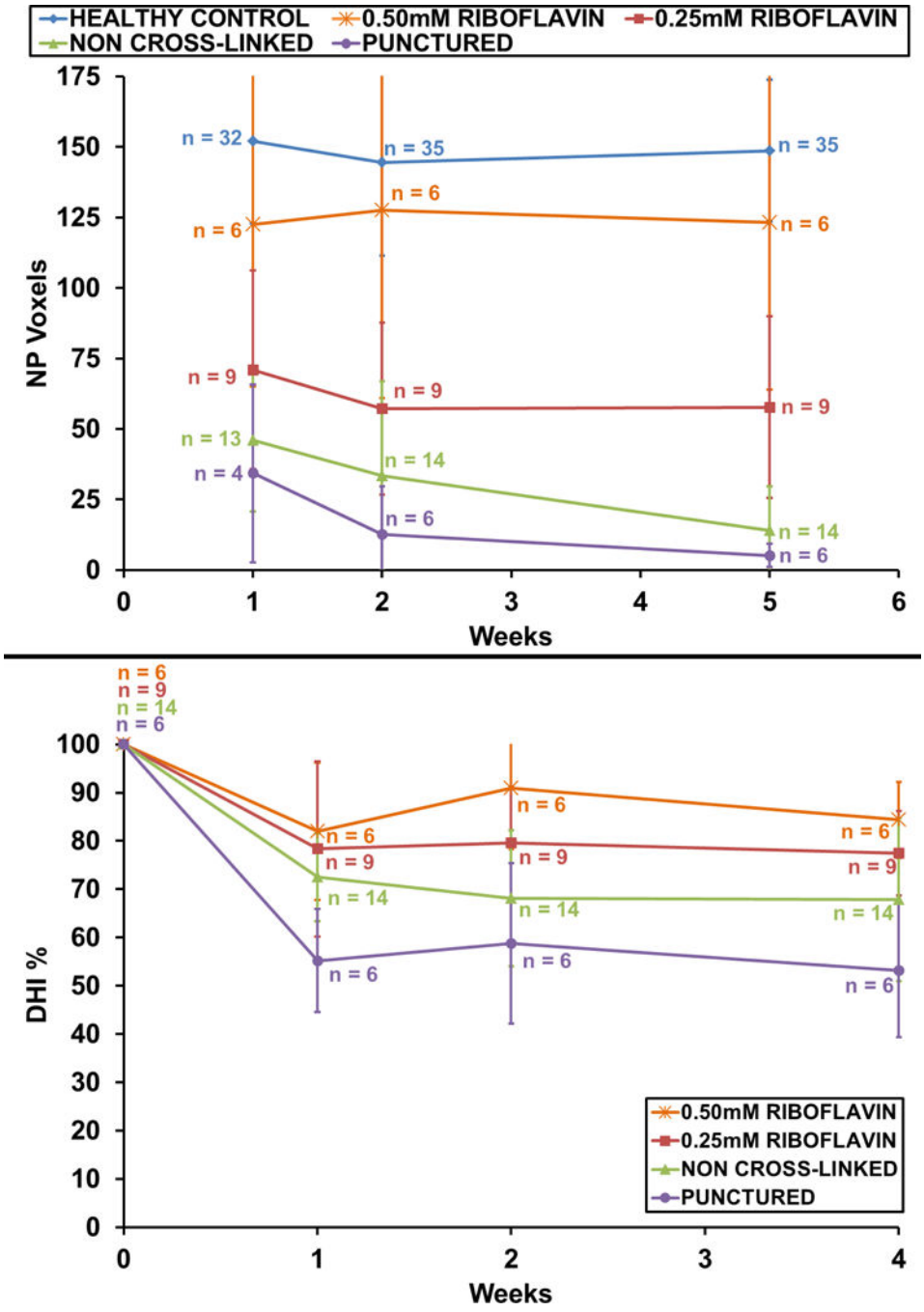

Fig. 3.

(A) Nuclear size according to NP voxel count measurements. The 0.5mM group showed slightly fewer NP voxels than did healthy discs over 5 weeks. Voxel counts of both cross-linked groups remained constant between the 2nd and 5th weeks. Animals injected with uncross-linked collagen gel showed a continuous drop in NP voxels over 5 weeks. The untreated group showed the lowest voxel count numbers at all time points. **(B)** Disc height measurements correlated with NP voxel count results. The 0.5mM group retained 88% of its

initial disc height; the untreated group dropped to 55%. Variations in n within groups resulted from MRI scheduling constraints.

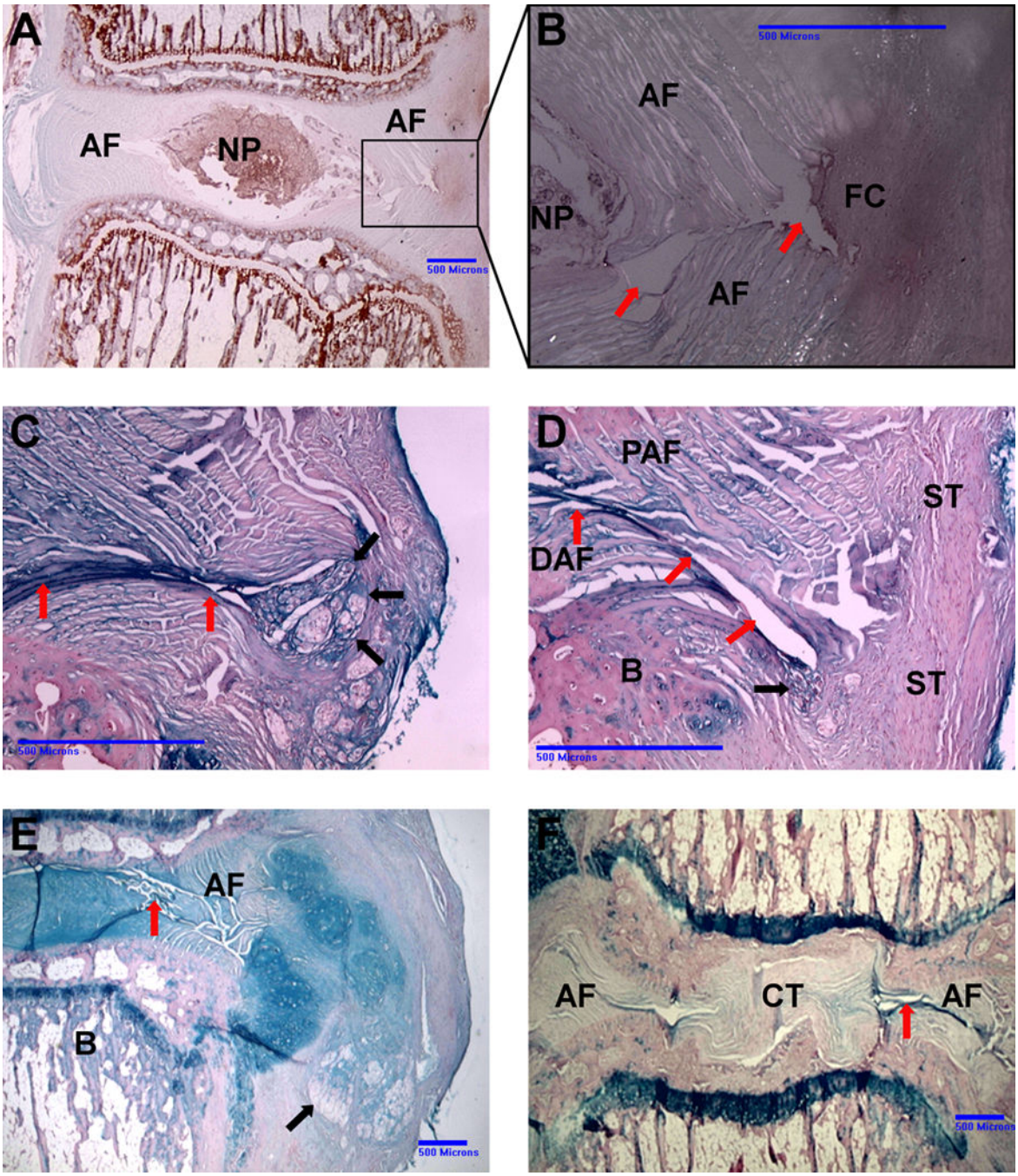

Fig. 4.

Different histological outcomes of punctured IVDs after five weeks. **(A)** Safranin O stain, **0.25mM RF group**. The disc displays an ovular NP of standard size. The needle-puncture defect and fibrous cap are outlined by the box. **(B)** Higher magnification under polarized light. The needle-puncture defect is clearly visible (red arrows). The inner 2/3 of the AF lamellae remain separated; there is no sign of tissue repair. The outer 1/3 of the defect is bridged by a fibrous cap (FC). The non-birefringent FC matrix appears to infiltrate the bright, birefringent AF fibers. **(C)** Alcian blue stain. **0.25mM RF group**. Only a thin fibrous

string (black arrows) bridges the annular defect (red arrows). **(D)** Alcian blue stain. **Uncross-linked group**. No fibrous tissue visible repairing the defect (red arrows). Distal annular fibers (DAF) and proximal annular fibers (PAF) remain separated and infiltrate the surrounding scar tissue (ST). The black arrow points to sequestered NP material. B indicates endplate bone. **(E)** Alcian blue stain. **Uncross-linked group**. NP tissue (black arrow) extrudes through the annular defect into the paravertebral space. The AF shows multiple fissures (red arrow). **(F) Untreated control IVD**. Needle-puncture defect (red arrow) induced severe degenerative changes. There is no organized AF tissue visible; the NP has been replaced with connective tissue.

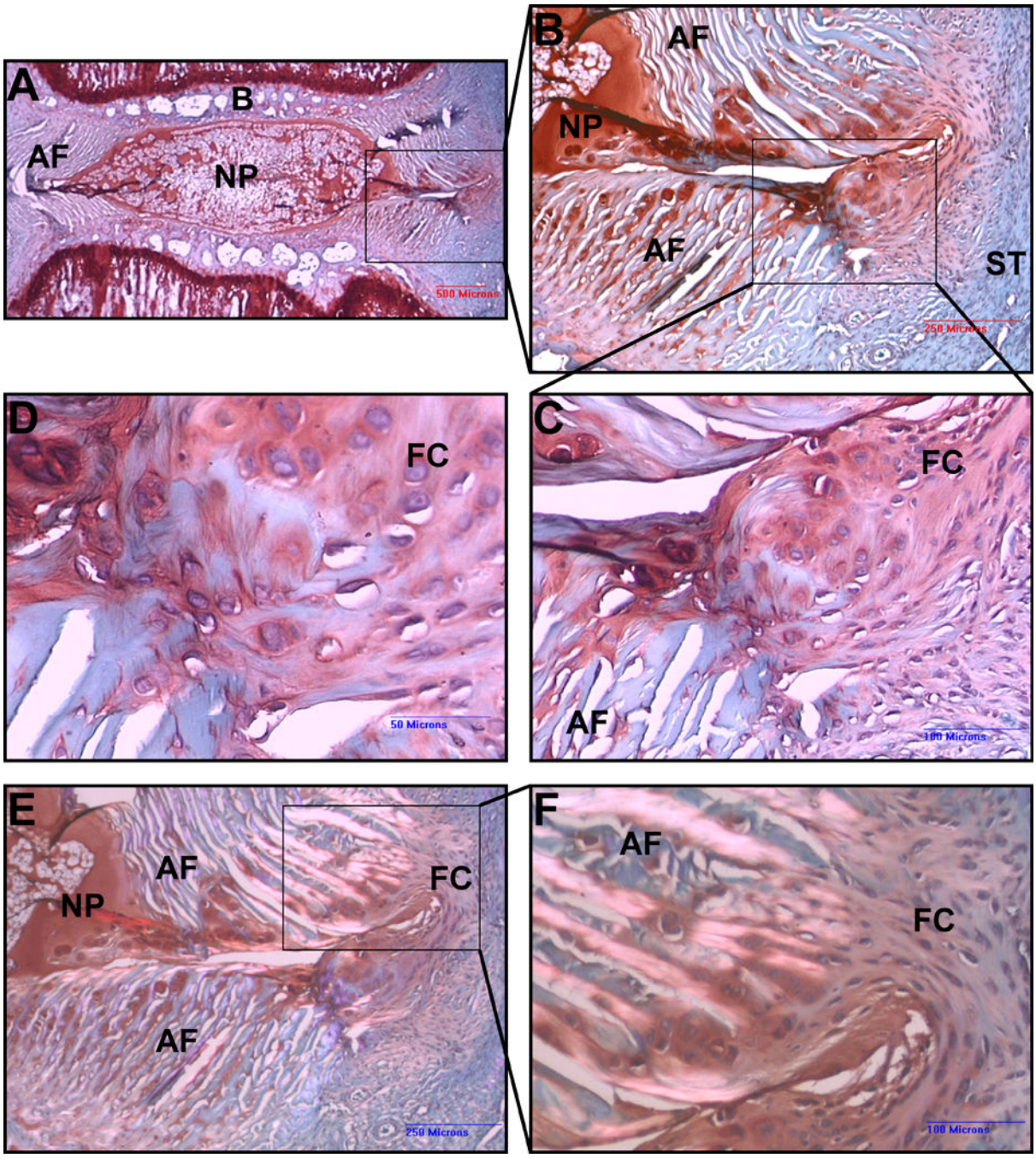

Fig. 5.

Safranin O stain. Punctured IVD, 0.5mM RF group after 5 weeks. (**A**) Low magnification. The NP displays standard size and ovular shape. A clear border separates the NP from the AF and endplate bone B. The box marks the needle puncture defect. (**B**) Higher magnification shows the needle puncture defect piercing through every layer of the AF. A fibrous cap, marked by the box, bridges the annular defect at the outer portion of the AF. The matrix of this fibrous tissue stains more intensely with Safranin O than does the surrounding scar tissue (ST). **(C), (D)** Higher magnification of the fibrous cap, which

appears to be infiltrating AF fibers. **(E), (F)** Same specimen as in A–C, viewed under polarized light. The bright birefringent AF fibers mesh with the non birefringent tissue of the fibrous cap.

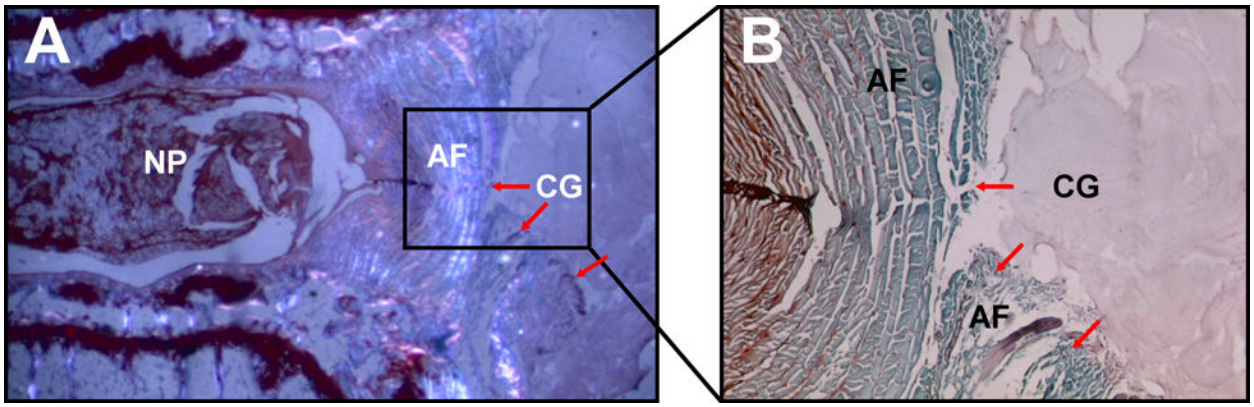

Fig. 6.

Fate of the collagen gel. **(A)** Safranin O stain, polarized light immediately after collagen gel (CG) injection. HDC distributes in the paravertebral space, covering the AF defect. In contrast to the AF, HDC is non birefringent under polarized light, indicating a lower tissue organization. **(B)** Higher magnification. The puncture defect is visible (red arrows). CG appears as an amorphous homogenous tissue which stains slightly positive for Safranin O. It does not migrate into the AF defect.

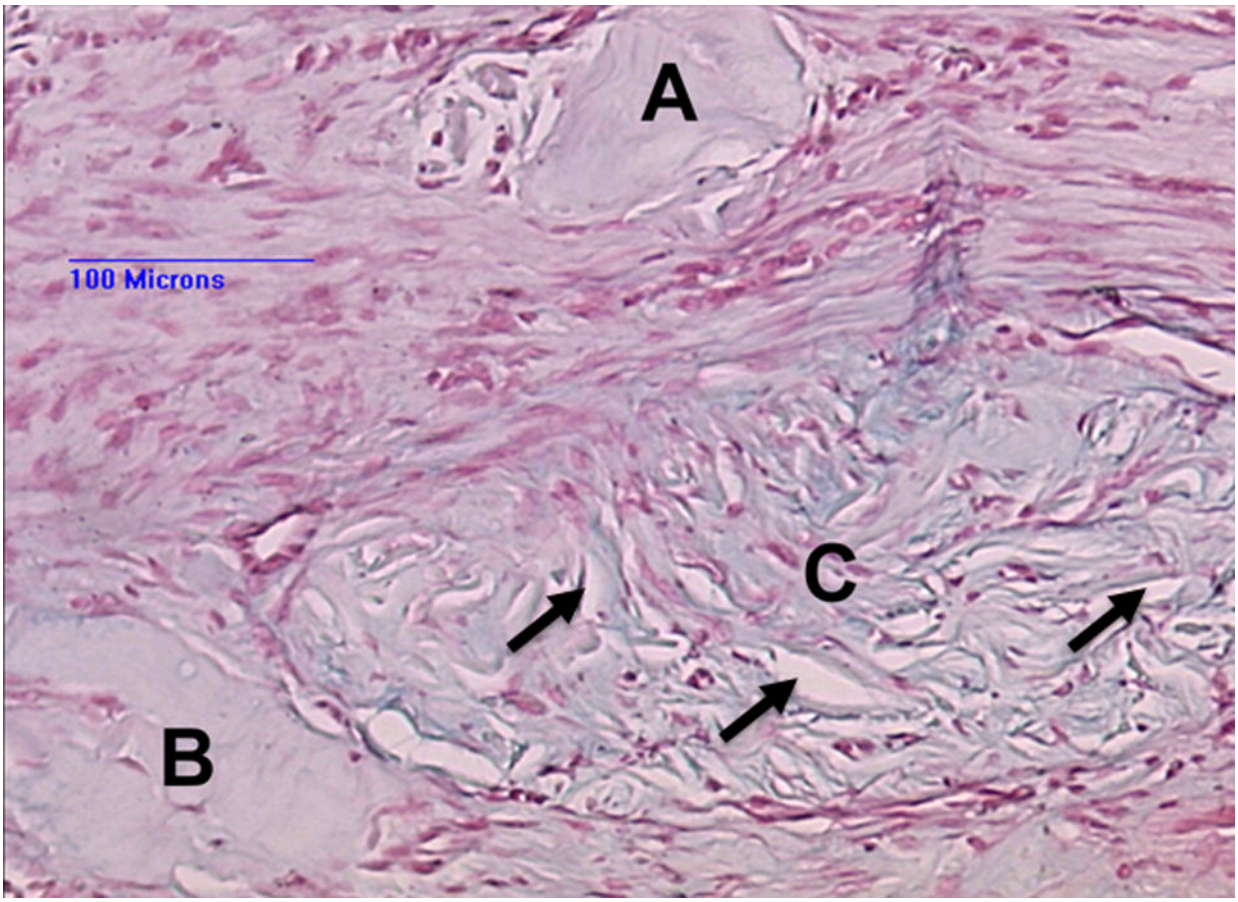

Fig. 7.

Fate of the collagen. Alcian blue stain. Paravertebral space 5 weeks after collagen injection. Three islets of amorphous homogenous collagen surrounded by scar tissue. Islet **A** shows no cell infiltration, islet **B** very limited. Islet **C** shows a high degree of fibroblast infiltration. The cells appear to reorganize the tissue, as indicated by resorbtive zones (black arrows) within the collagen tissue. There is no sign of an inflammatory response.